UNIVERSITATEA **POLITEHNICA** DIN BUCUREŞTI

Facultatea deINGINERIE MECANICĂ ȘI MECATRONICĂ
Departamentul de Organe de Mașini și Tribologie

No. CSUD Decision 646 from 10.03.2021

TEZĂ DE DOCTORAT

CERCETĂRI PRIVIND EFECTUL AMORTIZĂRII HISTERETICE ASUPRA FENOMENULUI DE OBOSEALĂ PRIN VIBRAȚII A LIPITURILOR DE TIP Sn-Ag-Cu UTILIZATE ÎN APARATURA ELECTRONICĂ

RESEARCH ON THE EFFECT OF HYSTERETIC DAMPING ON THE PHENOMENON OF VIBRATION FATIGUE OF Sn-Ag-Cu TYPE SOLDERS USED IN ELECTRONIC EQUIPMENT

Autor: Eng. Alina-Maria PETRESCU (Stoica)

Conducător de doctorat: Prof.dr.eng. Andrei TUDOR

DOCTORATE COMISSION

President	Prof. dr.eng. Radu CHIRIAC	from	University Politehnica of Bucharest
Scientific coordinator	Prof. dr.eng. Andrei TUDOR	from	University Politehnica of Bucharest
Reviewer	Prof.dr.eng. Spiridon CREȚU	from	Technical University „Gheorghe Asachi” of Iași
Reviewer	Prof.dr.eng. Lorena DELEANU	from	University „Dunărea de Jos” of Galați
Reviewer	Conf.dr.eng. Ioan PLOTOG	from	University Politehnica of Bucharest

BUCHAREST

2021

CONTENT

Words of thanks

Concluding this stage of my life, I would like to thank first of all the doctoral supervisor prof. dr. eng. Andrei TUDOR for the careful scientific guidance and for all the support given during the entire period of elaboration of the doctoral thesis. I would like to express my sincere gratitude for the teacher's advice, understanding and patience.

I want to express my gratitude to the members of the steering committee, for the support provided, the advice and last but not least, the time given for the entire duration of the studies. I thank Mr. prof. dr. eng. Sorin CĂNĂNĂU, Mr. prof. dr. eng. Alexandru Valentin RĂDULESCU and Mrs. lect. dr. eng. Georgiana Ionela PĂDURARU.

Thank you from the bottom of my heart, with great gratitude, to all the members of the doctoral committee, to prof. dr. eng. Spiridon CREȚU from the Technical University "Gheorghe Asachi" from Iasi, to prof. dr. eng. Lorena DELEANU University „Dunărea de Jos” of Galați and Mr. Assoc. Ioan PLOTOG from the University POLITEHNICA of Bucharest for the patience and goodwill with which they analyzed the thesis.

Countless thanks for the warmth with which they received me and with all the technical support they gave me, to the gentlemen from UPB CETTI ITA, lect.dr.eng. Bogdan MIHĂILESCU and Mr. teh. Teodor MIHĂILESCU.

Sincere thanks to the entire staff of the Department of Machine Elements and Tribology who was with me and supported me throughout this period. I would like to thank in particular Mrs. and so lect. dr. eng. Georgiana Chișiu for all the advice and guidance she gave me on the thesis but also on the didactic side and last but not least for her friendship. Heartfelt thanks to prof. dr. eng. Adrian PREDESCU for his support and all his trust. I would also like to thank technician Mihai ROZOREA for his technical support and promptness. I would also like to thank some dear people who have helped and guided me since I was a bachelor, mrs. associate professor Irina RĂDULESCU and prof. dr. eng. Alexandru Valentin RĂDULESCU. The whole department was with me with understanding and patience, and in this way I want to thank mrs. and so lect. dr. eng. Marilena STOICA for the technical support provided and last but not least to prof. dr. eng. Petre Lucian SEICIU. Thanks also go to Mr. assoc. prof. dr. eng. Radu-Mircea CARP-CIOCÂRDIA for the trust he had in me on the teaching side and for his support. I would also like to thank assoc. prof. dr. eng. Radu MIRICĂ for all the useful advice and support.

I thank my parents, grandparents and sister for the love, for all the education I received and for all the sacrifices they made for me to get to where I am now. With special love I want to thank my husband, Nicolae-Alexandru STOICA, who was with me throughout the thesis, at all times good and in the worst, I thank him for his love, support and all the patience he had with me is a wonderful man.

In conclusion, I would like to thank all the wonderful people and friends who trusted me and those who helped and encouraged me directly or indirectly to complete the thesis.

KEY WORDS

Indentation method, hysteretic damping, fatigue deterioration phenomenon, lead-free solder alloys, reliability of solders in electronics, vibrations of electronic components.

SINTHETIC PRESENTATION OF THE CHAPTERS OF THE DOCTORAL THESIS

Chapter 1 entitled "*Current state of research on soldering used in electronics*" presents generalities on lead-free solder alloys. The most widely used alloy used in the electronics industry is Sn-Ag-Cu, which has several major benefits compared to other alloys: good mechanical properties, stable interfaces with several metal substrates or surface finishes, it is not toxic to the human body. There are also disadvantages regarding this soldering alloy such as the slightly higher degree of melting, the slightly higher hardness and the appearance of solidification and formation defects [1], [2]. At the same time, the characteristics of the printed wiring board (PCB) assembly that is used to create a connection between components are also presented. This becomes an electrical circuit when the electronic components are planted in the solder paste deposits made on the surfaces dedicated to making connections (forests) on the surface of the printed wiring board in figure 1.1.a. This whole assembly is called the printed wiring board assembly represented by figure 1.1.b.

a. 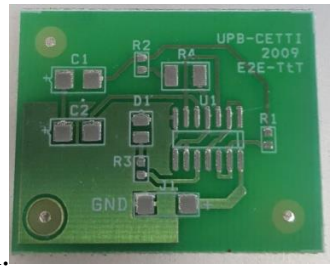

b. 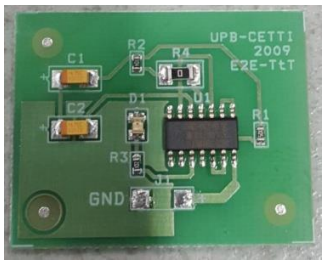

Figure 1. 1. ***Exemple of a. PCB and b. Assembly PCB***

Typically, the rigid supports of PCBs are: Flame Retardant-2, Flame Retardant-3, Flame Retardant-4, Composite Epoxy Materials-1, Composite Epoxy Materials-3 [24]**.**

Also in this chapter are highlighted the methods of mounting electronic components as follows [2]: Through Hole Technology, Insert mounting combined with single-sided surface mounting, Surface Mount Technology only, surface mounting on both sides, surface mounting on both sides combined with insert mounting.

The finishing of the conductive surfaces of the printed wiring boards forms a critical interface between the component and the interconnection circuit. There are several types of surface finishes: Hot Air Solder Level, Non-electrolytic nickel deposition / Gold immersion (Electroless Nickel Immersion Gold), organic solder preservation (Organic Solderability Preservative).

The soldering technology of the components is the gluing in the state of vapor, a technology that uses the condensing heat of a working fluid to remel the solder paste in order to obtain a joint (gluing).

This chapter develops the reliability part of the solders used to make electronic connections which depends on the integrity of the structural interconnections made on the surface of the printed wiring board by the joints made after the soldering process.

Defective mechanisms due to vibrations being: rupture of component terminals due to fatigue, failure due to structural fatigue, failure due to solder fatigue [39].

Objectives of the thesis

Based on the bibliographic study on the reliability of SnAgCu type welds (SAC) and Cu layers, this doctoral thesis aims at the following objectives:

- identification of the mechanical properties of SAC type materials with significant influence on the phenomenon of mechanical fatigue,

- evaluation of the state of stresses and deformations at the contact of a spherically connected conical penetrator, with the plate covered with electrically conductive layers, and of the SnAgCu type solders used in the electronic equipment,

- theoretical and experimental determination of hysteretic damping of copper layers and SnAgCu type welds with the penetration method,

- study of the creep behaviors of SnAgCu type welds,

- analysis of the rigidity of the soldering system - component on the plate,

- equivalence of cycles of random variable stresses according to the criterion of stored internal energy (hysteresis phenomenon),

- determining the durability of the connection terminals and SnAgCu solders on plates with random vibrations.

Chapter 2 entitled “Analysis of the phenomenon of hysteretic damping of Sn-Ag-Cu type solders and of the copper-plated support plate” proposes an analysis of the state of stresses and deformations at the contact of a conical penetrator with the spherically connected tip with a plate used in electronics industry. On the plate are deposited 2 layers on which are glued electronic parts with lead-free solder alloys. Indentation aims to determine the parameters of elasticity, hardness, creep characteristics of the layers and the hysteretic damping coefficient. The scheme of the conical penetrator with spherically connected tip is shown (Figure 2.1), where the geometry of the cone is evaluated by the semicircle α and the connection radius R_c, the cone being considered rigid, the layers c_1 and c_2 are elastically and plastically deformed, depending on the normal load F_n and the elastic characteristics of the two materials 1 and 2.

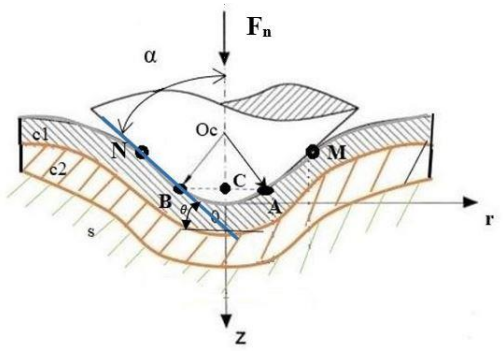

Figure 2. 1. **Scheme of the contact between the conical penetrator and the covered plate**

Starting from the equation of the profile of the penetrator in the contact area with the plate, which is written as a function of the angle of attack of the cone $\theta = (\pi/2) - \alpha$ and the sphere-sphere separation radius (b), deducing an equation simplified profile, determine the exact profile of the contact curve that has the shape:

$$z_{ae}(r_a) = \begin{cases} -1 + \sqrt{1 - r_a^2} \ , & for \quad 0 \le r_a \le sin\theta \\ r_a tg\theta + 1 - cos\theta - sin\theta \ tg\theta \ , & for \ sin\theta < r_a \le a_a \end{cases} \tag{2.3}$$

with $a_a = a/R_c$ cone radius in the area separating the penetrator from the deformed material.

By dimensioning the force for the exact profile (P_{ae}) and, similarly, for the approximate profile (P_{ae}) and the elastic penetration limit forces are determined only for the spherical area, and in Figure 2.4 we can see the graphical representation of the normal dimensionless limit forces for the exact penetrator (P_{ael}) and for the approximate one (P_{al}) as a function of the angle of attack of the cone θ in radians. It is observed that the differences between the limit forces, different on the spherical area, for the exact penetrator and for the approximate one, are very small.

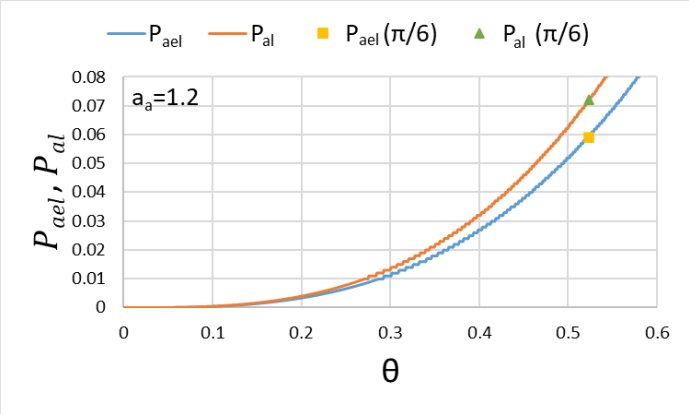

Figura 2. 4. ***Forța elastică limită pentru zona sferică***

Defining the penetration as (2.19), where ϕ_s is the contact angle between the sphere and the elastic half-space, it is observed in figure 2.5 that the effect of the angle of attack θ is very small on the penetration of the cone in a fairly wide range of dimensionless forces:

$$\delta_{as} = \frac{\delta}{R_c} = 1 - \cos(\phi_s) \quad , \tag{2.19}$$

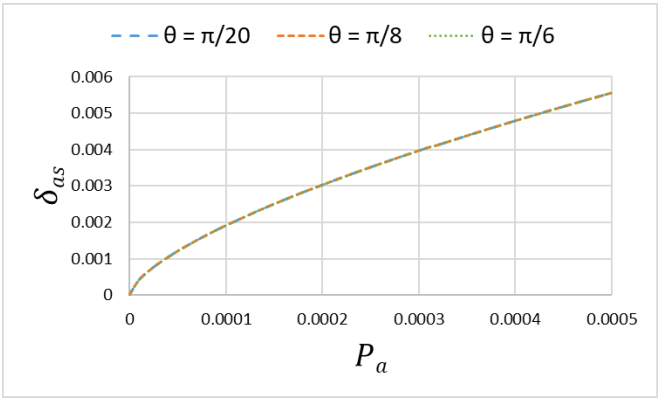

Figura 2. 5. ***Penetration of the cone in the sherical area***

In the final part, determine the total relative penetration (sphere, cone) δ_{ac} as a function of loading (P_a) and the angle of attack of the cone (θ).

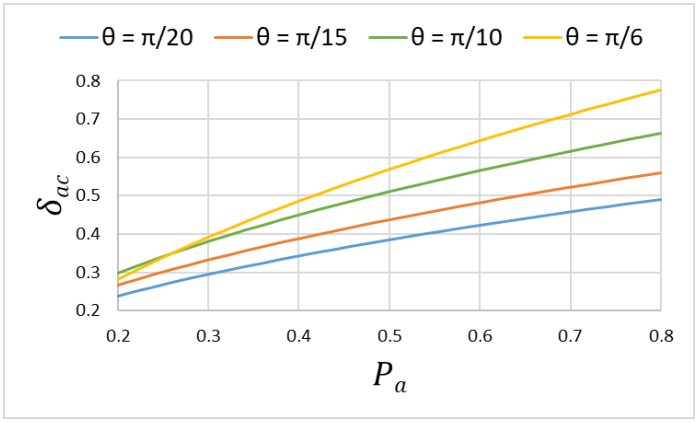

Figura 2. 6. ***The total penetration of the cone***

For the case of pressure distribution, the effects of the load for an angle of attack on the pressure distribution on the contact surface were highlighted, as can be seen in Figure 2.8.

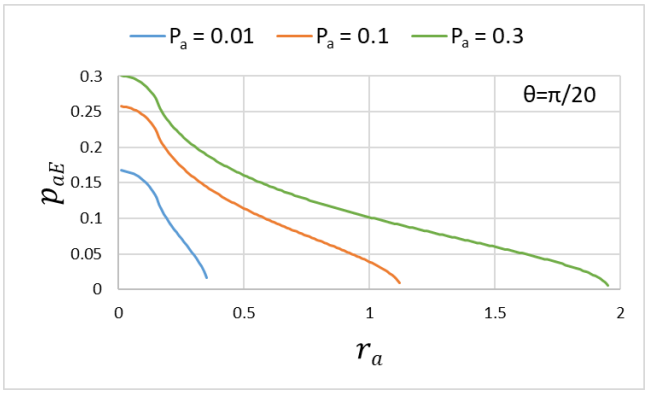

Figure 2. 8. ***Distribuția de presiuni pe suprafața de contact funcție de încărcare***

Taking into account the rigidity of the contact of the cone with the elastic half-space, for the stiffness analysis the approximate shape of the penetrator is used, and if we dimensionize the stiffness formula, by eliminating the angle φ_0 between force and penetration, the dimensionless stiffness with $F_c(\theta, \varphi_0)$:

$$c_{an} = \frac{dP_a}{d\delta_a} = \frac{1}{\pi R_c E_r} \cdot \frac{dP}{d\delta} = \frac{c_n}{\pi R_c E_r} = F_c(\theta, \varphi_0)\,, \tag{2.37}$$

Presented in Figure 2.9, the function of normal dimensionless rigidity, obtained numerically.

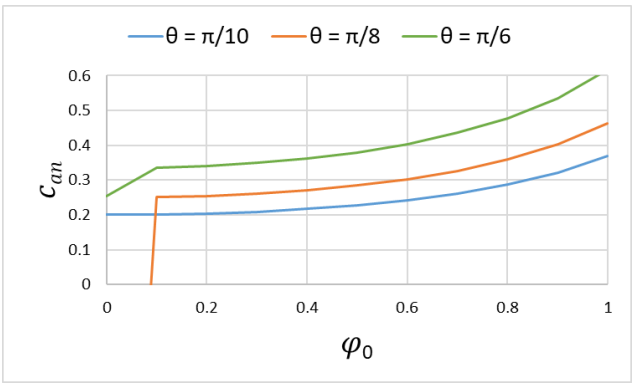

Figure 2. 9. ***Rigiditatea normală adimensional a stratului cu penetrator conic racordat sferic***

For the contact in the spherical area of the penetrator, Hertz's theory is applied, initially considering the layer as an elastic half-space and determining the displacements on the contact surface [63], [66] in the z direction and in the radial direction inside the contact circle, outside contact circle. The stresses on the contact surface (inside the contact circle and outside the contact circle), the stresses in the half-space in the z direction and the main tangential stress τ_1 which has the maximum value below the contact surface (inside the half-space) are also determined.

In order to generalize the results regarding the displacements and tensions in the spherical area of the penetrator, the main sizes are dimensioned, and in figure 2.10 the dimensionless displacements from the half-space on the contact surface are presented.

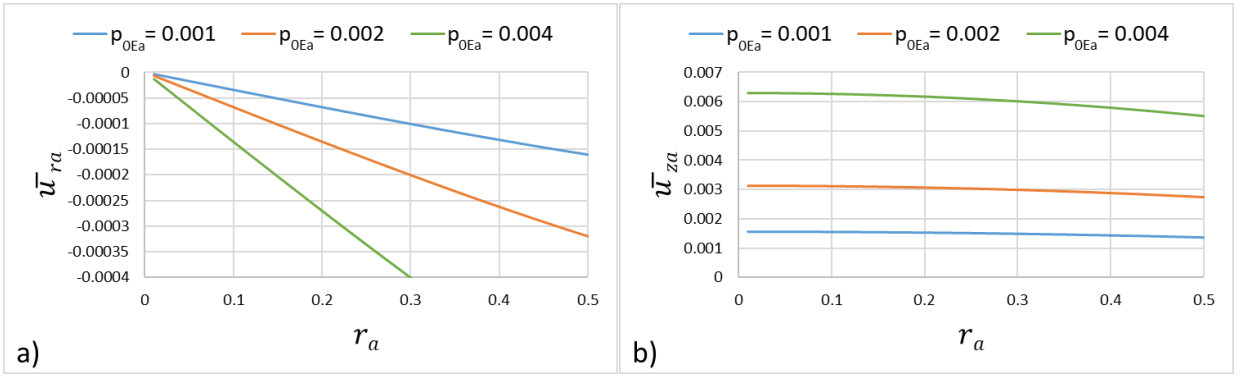

Figure 2. 10. ***Radial displacements on the spherical surface of the penetrator (a) and in depth (b)***

Define the energy stored at the load (W_{ep}) which is the area under the load curve, while the energy released at the discharge (W_p) is below the discharge curve, which is also shown in Figure 2.20. The total energy losses by hysteresis are calculated as $W_{ep} + W_{cr} - W_p$.

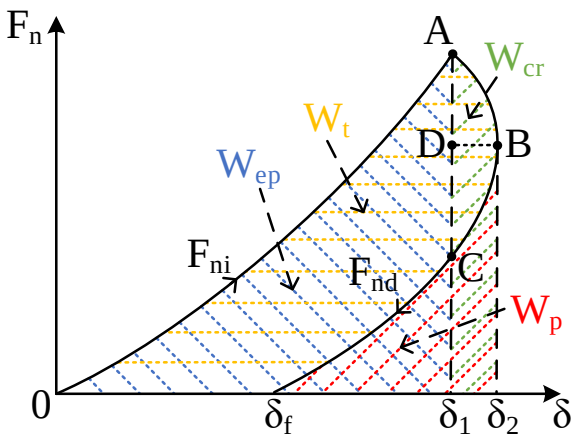

Figura 2. 20. ***Schematic diagram of the creep indentation process***

The dimensionless mechanical work on loading results:

$$W_{epa} = \frac{W_{ep}}{\pi R_c^3 E_r} = \int_0^{\delta_1} P_{ai} d\delta_a, \tag{2.75c}$$

where P_{ai} is the dimensionless force at loading and which depends on the state of deformation and the area of contact of the penetrator with the material.

Figure 2.21 illustrates the dimensionless mechanical work for loading different materials, evaluated by the specific flow resistance.

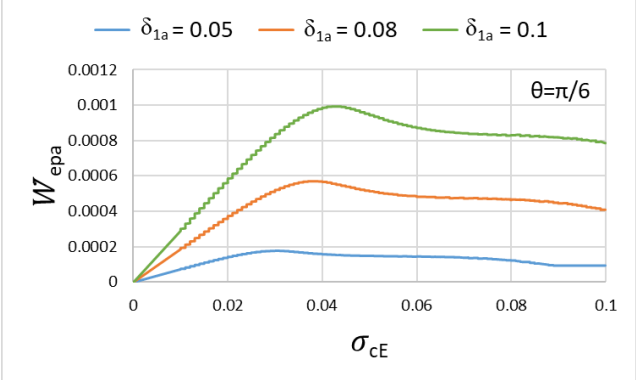

Figure 2. 21. ***Lucrul mecanic la încărcare pentru diferite materiale***

The correlation force (F_n) - displacement (δ) at discharge is estimated with the Sneddon method [63], according to which, for the penetrator of the form $z = B \cdot r^n$ (polynomial function) (B and n are constant, and z- ordinate , r- abscissa) and making the necessary dimensions, is shown in Figure 2.23 force dependence - displacement at discharge for penetration with different spherical peaks (n).

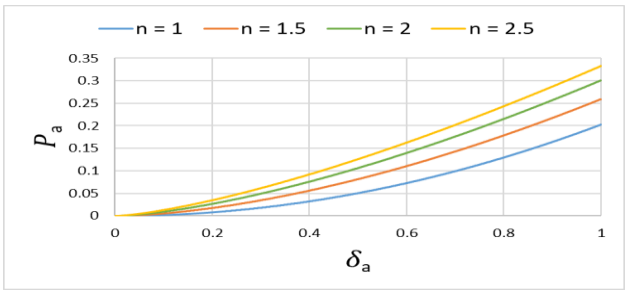

Figure 2.23. ***Theoretical penetrator discharge curve with different shapes***

Figure 2.25 shows the mechanical work on discharge for different plastic penetrations (δ_{fa}) and angles of attack (θ).

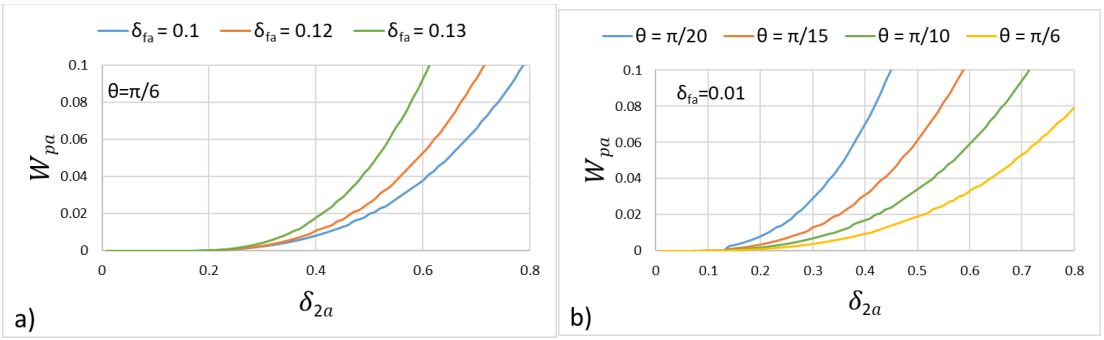

Figure 2.25. ***Theoretical mechanical work of unloading for different plastic penetrations (a) and angles of attack (b)***

By dimensioning, the mechanical work during creep has the expression:

$$W_{cra} = \begin{cases} 2\Phi_{sfe}\left\{\left(\delta_{2a}-\delta_{fa}\right)^{3/2}\left(\delta_{2a}-\delta_{1a}\right)-\frac{2}{5}\left[\left(\delta_{2a}-\delta_{fa}\right)^{5/2}\left(\delta_{1a}-\delta_{fa}\right)^{5/2}\right]\right\} \\ for\ 0 \le \delta_{2a} \le 1-cos\theta \\ 2\Phi_{cone}\left\{\left(\delta_{2a}-\delta_{fa}\right)^{2}\left(\delta_{2a}-\delta_{1a}\right)-\frac{1}{3}\left[\left(\delta_{2a}-\delta_{fa}\right)^{3}\left(\delta_{1a}-\delta_{fa}\right)^{3}\right]\right\} \\ for\ \delta_{2a} > 1-cos\theta \end{cases} . \quad (2.84)$$

Figure 2.27 shows the evolution of mechanical work during the creep period for different plastic penetrations and cone angles.

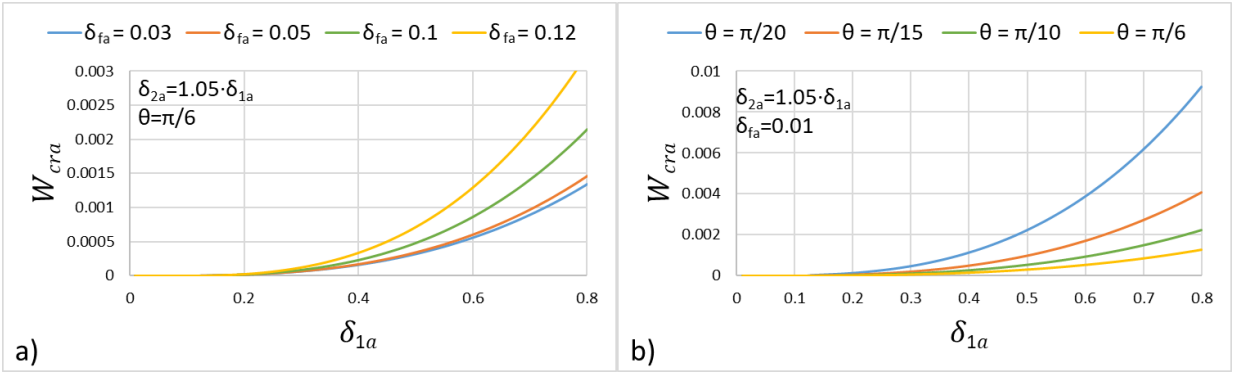

Figure 2.27. ***Mechanical creep work depending on the maximum force penetration (δ_{1a}) for different plastic deformations (a) and cone angles (b)***

Total mechanical work at a loading-unloading in dimensionless coordinates:

$$W_{ta} = \frac{W_t}{\pi R_c^2 E_r} = W_{epa} + W_{cra} - W_{pa}, \tag{2.85b}$$

The coefficients of total losses (β_h),), creep (β_{cr}) and plastic deformation (β_p) are defined.

$$\beta_h = \frac{W_{ta}}{W_{epa} + W_{cra}},\ \beta_{cr} = \frac{W_{cra}}{W_{epa} + W_{cra}}\ ,\ \beta_p = \frac{W_{pa}}{W_{epa} + W_{cra}}, \tag{2.86}$$

The differences between the exact profile of the penetrator and the approximate one are small for small angles of attack.

Based on the equations of the force-deformation curves, the energy stored in the material during loading, the creep energy and the recovered elastic energy are determined and the specific hysteresis coefficients are determined.

In Chapter 3 entitled "*The phenomenon of fatigue deterioration of the copper layers of SnAgCu type solder joint*" it is proposed to apply a deterioration model based on the evaluation of the hysteresis curve, obtained from experimental penetration tests with cone-type penetrator with spherically connected tip. The basic model (E-P) analyzes the total service life (number of cycles N_f) and is completed with the phenomenon of deterioration on load cycles (load-bearing area and damping coefficient). As an example, emphasis is placed on the significant change in the modulus of elasticity with the number of Sn-Pb solder stress cycles tested experimentally in the works [83]–[85].

Using the energy partitioning model (EP) determines the number of cycles to deterioration (N_f)) which contributes to establishing the total damage equation determined by superimposing damage by plastic deformation (D_p) and creep (D_{cr}) by the number N cycles:

$$\frac{D}{D_c} = \frac{D_P + D_{cr}}{D_c} = \left(\frac{N}{N_{fp}}\right)^{\eta_p} + \left(\frac{N}{N_{fcr}}\right)^{\eta_{cr}}, \tag{3.15}$$

where N_{fp} is the number of cycles for damage only by plastic deformations, N_{fcr}- the number of cycles for damage only by creep, η_p and η_{cr} are experimentally determined empirical exponents. For the evaluation of the exponent η_p, experimental determinations are made at different inelastic deformations. For the tested SAC materials, the exponent $\eta_p \approx 0{,}47$. The decrease of the stresses with the number of cycles at high temperatures and low deformation speeds, allows the determination of the exponent η_{cr}. The average value of this exponent is $\eta_{cr} = 0{,}52$.

The degradation (D) is determined to be (3.16), and figure 3.5 exemplifies the degradation with the number of stress cycles N, for values of the number of cycles of deterioration by plastic deformations (N_{fp}) (a) and different cycles of deterioration by flow (N_{fcr}) (b).

$$D = 0{,}5\left(\frac{1}{N_{fp}}\right)^{0{,}47} \cdot N^{0{,}47} + 0{,}5\left(\frac{1}{N_{fcr}}\right)^{0{,}52} \cdot N^{0{,}52} = \\ = C_1 \cdot N^{0{,}47} + C_2 \cdot N^{0{,}52}, \tag{3.16}$$

where N_{fp} și N_{fcr} depend on the load (speed and amplitude) and temperature. The constants C_1 and C_2 depend on the test conditions.

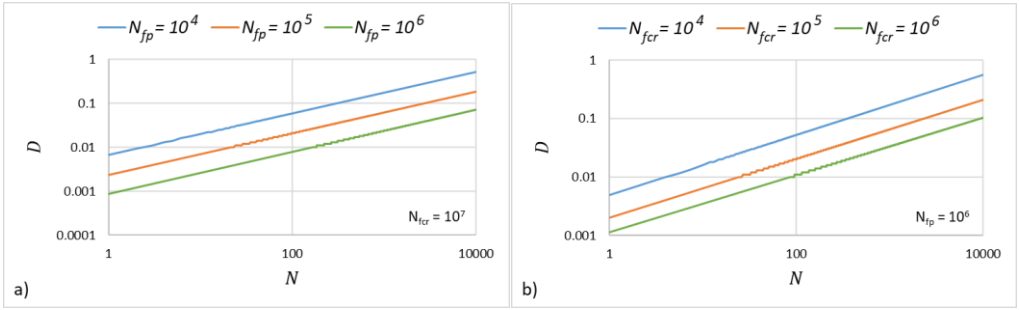

Figure 3. 5. ***Damage to material 95,5%Sn-5,9%Ag-0,6%Cu for various critical numbers of plastic cycles (a), creep (b)***

The constitutive equation of the solder alloys of electronic components changes with the number of stress cycles. At any time of stress, four modes of deformation appear in the solder [88]. For example, for a solder subjected to tangential stresses (τ), the deformations are: elastic deformation γ_e (Hooke's law is accepted), independent of time, plastic deformation γ_{pl} (accept the power function), independent of time, deformation of primary creep γ_{pcr} (exponential model is accepted), dependent on deformation velocity, secondary creep deformation γ_{scr}, dependent on deformation velocity.

The total deformation is given by the relation (3.17), and the constitutive equation of the solder material is obtained by replacing the coefficients of the equation:

$$D = \gamma_e + \gamma_{pl} + \gamma_{pcr} + \gamma_{scr}. \tag{3.17}$$

Analyze the evolution of the constitutive equation for SAC type materials (95.5Sn-5.9Ag-0.6Cu), deduced by Zhang 2009 [88].

Modulul de elasticitate longitudinal scade o dată cu creșterea numărului de cicluri de solicitare.

The energy partition (E-P) in the charging cycle is accepted as a constitutive property of solders. For the elastic deformation within the constitutive equation of the soldering alloys, Hooke's law is applied, and for the plastic deformation, the exponential model is accepted.

Chapter 4 entitled “Experimental results on the mechanical behavior of SAC solders and copper plated backing plate” presents indentation tests, creep indentation tests and scratch tests that help determine the hysteretic damping coefficient, determination of the energies stored in the alloy gluing and coating and characterizes the type of material.

The experimental determinations in this thesis were made with the help of the CETR UMT Multi-Specimen Test System tribometer, from the Department of Machine Organs and Tribology, from University “POLITEHNICA” of Bucharest. The 120 ° peak angle and 200 mm radius with a capacitive sensor are shown in Figure 4.1.

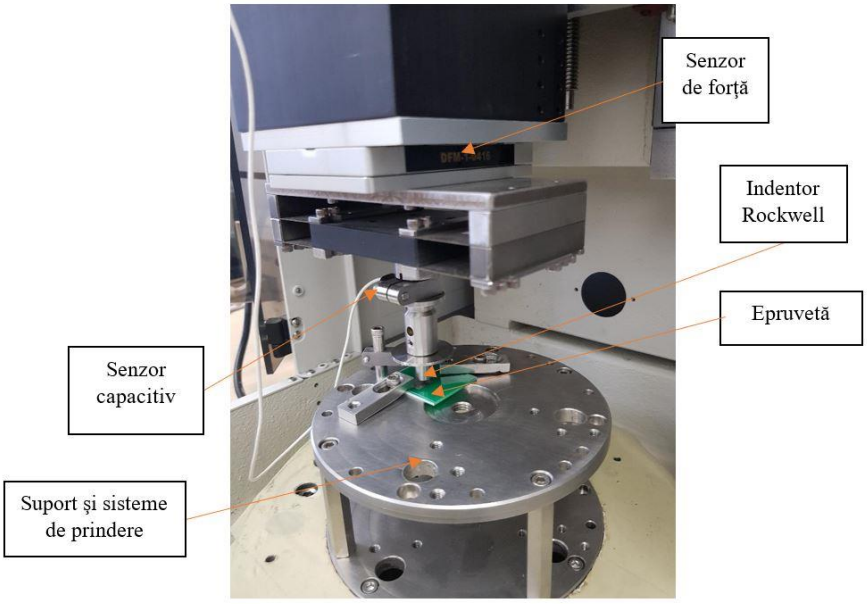

Figure 4. 1. ***Testing equipment***

For the part of making the specimens, it should be mentioned that the connection between the terminal of the electronic component and the pads of the interconnection structure is made with the help of solder paste SAC 305 (96.5% Sn / 3.0% Ag / 0.7% Cu) . The deposition of the solder paste was done by manual printing using the LPKF ZelPrint LT300 equipment, which is used for the deposition of the solder paste of surface mounted components (SMT). The stainless steel template used is 200 μm thick.

In the analysis of the behavior of the solder alloy SAC 305 in indentation tests, three loading forces were used: 3 N, 5 N and 7 N respectively, and in figure 4.6 we can see the graphical representation of the loading force depending on the depth penetration corresponding to the loading force of 3 N. The visco-elasto-plastic behavior of the material was analyzed based on the force-strain diagram.

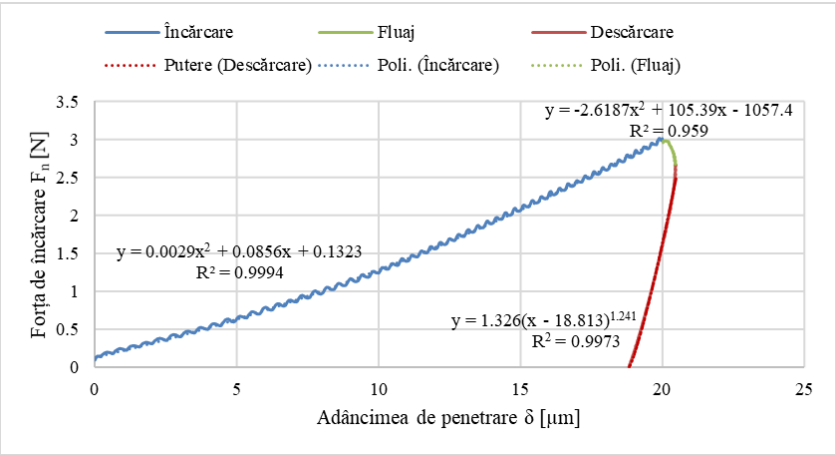

Figure 4. 6. ***Graphical representation of the load force (F) of 3 N as a function of depth (δ) at indentation***

The following were determined: the deformation at the end of the loading period (δ_1), the maximum deformation caused by the creep occurring at the beginning of the unloading period (δ_2) and the plastic deformations (δ_f) and the elastic deformations ($\delta_e = \delta_2 - \delta_f$) of the solder alloy SAC 305 for the three load forces are shown in Table 4.1.

Table 4. 1. ***Indentation test results***

Loading force [N]	***H*** [GPa]	$\boldsymbol{\delta_1}$ [μm]	$\boldsymbol{\delta_2}$[μm]	Plastic deformation ($\boldsymbol{\delta_f}$) [μm]	Elastic deformation ($\boldsymbol{\delta_e}$) [μm]
3	**0,1105**	**19,999**	**20,472**	**18,813**	**1,659**
5	0,1287	29,223	29,913	27,776	2,137
7	**0,1334**	**38,478**	**39,509**	**36,401**	**3,108**

The loading curves and the creep curves are calculated as a polynomial function of degree 2 : $F_n = x\delta^2 + y\delta + z$, and the discharge curve as a function of shape power $F_n = \alpha_c(\delta - \delta_f)^{m_c}$.

To determine the total energy losses by hysteresis in the indentation process (W_t), it is necessary to determine on the basis of the diagrams force - deformation, energy stored in the material during loading, energy stored during creep and energy released during download. These energies are presented in table 4.3.

Table 4. 3. ***Hysteresis energy losses for SAC305 solder alloy in indentation tests***

$\boldsymbol{F_n}$ [N]	$\boldsymbol{W_{ep}}$ [N·μm]	$\boldsymbol{W_p}$ [N·μm]	$\boldsymbol{W_{cr}}$ [N·μm]	$\boldsymbol{W_t}$ [N·μm]	$\boldsymbol{\beta}$
3	**27,496**	**1,840**	**1,361**	**27,017**	**0,936**
5	65,395	3,876	3,428	64,947	0,944
7	**119,024**	**7,177**	**6,690**	**118,538**	**0,943**

Carrying out a statistical analysis of indentation tests (10 tests under the same conditions with a load force of 5 N), establishing the law of distribution of test results using the Kolmogorov-Smirnov test and analysis of functions for Gaussian distribution, exponential distribution and Weibull distribution, in the Mathcad 14 program, having a significance threshold α = 0.000001, with λ = 2.693, leads to the fact that the results are in accordance with the Gaussian and Weibull distribution law and can state that other experimental results will fit the thresholds determined in this subchapter with a probability of 99.27%.

Following the analysis of the behavior of the SAC 305 solder alloy in indentation creep tests, the visco-elasto-plastic behavior of the material can be determined. Creep indentation tests consist of three stages. The first stage and the last stage are identical to those of the micro-indentation tests, the difference between the two types of tests being made by the intermediate stage between them, in which the indenter was held at a normal constant load force of 3 N, 5 N and 7 N respectively for the three tests performed. The tests were performed at room temperature of 26 ° C.

Following the experiments, the maximum penetration for the indentation part δ_1 [μm], the maximum penetration depth after the creep period δ_2 [μm] and the plastic deformation δ_f [μm] and elastic δ_e [μm] corresponding to the three are recorded and determined. penetration forces F_n applied for a period of 120 minutes.

Table 4. 11. ***Energy losses from indentation creep tests***

Normal loading force [N]	W_{ep} [N·µm]	W_p [N·µm]	W_{cr} [N·µm]	W_t [N·µm]	β
3	**28,318**	2,206	**36,3**	62,412	**0,966**
5	**65,64**	4,988	**88,635**	149,287	**0,968**
7	**120,686**	8,703	**148,946**	260,929	**0,968**

To analyze the behavior of the SAC 305 solder alloy in scratch tests, two types of tests were performed: at variable depth 0 → 0,1 mm, 0 → 0,2 mm, 0 → 0,3 mm and at constant depth of 0,1 mm, 0,2 mm and 0,3 mm. All tests were performed at a length of 7 mm at a constant speed of 0.2 mm / sec for 35 seconds.

Following the scratch tests at variable depth, analyzing the evolution of the coefficient of friction, it is observed that for the test:

- 0 – 0,1 mm the relative coefficient of friction is constant throughout the test,

- 0 – 0,2 mm from a depth of about 0.09 mm the coefficient of friction begins to decrease (approximately from the middle of the test),

- 0 - 0,3 mm also at a depth of 0.09 - 0.1 mm it starts to decrease.

Analyzing the evolution of the acoustic emission (AE), a significant increase is observed in the case of tests at greater depth (0 - 0.3 mm and 0.3 mm). The increase of the acoustic emission level is due to the increase of the normal and the tangential force, but also to the penetration of the indentor in the Cu layer, respectively FR4.

At the same time, to determine the type of character of the material (ductile / brittle) was used the abrasiveness factor which has the following formula [89], [105], [106], [107]:

$$f_{ab} = 1 - \frac{(A_1+A_2)}{A_v}; \tag{4.9}$$

where (A_1 + A_2) represents the cross-sectional area of the created edges, Av represents the cross-sectional area of the wear trace.

Profiles of the marks left by the indentor after the tests were made and the abrasiveness parameter was determined for all scratches, where the visco-elasto-plastic behavior of the material can be observed, the material having a ductile character, resulting in values of the abrasiveness factor lower than 1.

In this chapter, indentation tests were performed on the support plate with copper layer and HASL type surface finish, at forces of 3 N, 5 N, 7 N. For each test, the force-strain diagram was drawn. established the deformations, determined the constants of the power and polynomial functions of degree 2 and determined the energies and the hysteretic damping coefficient of the material. Following the experimental results, it is found that the energies have an exponential increase with the charge, only the creep energy has a lower variation. The hysteretic damping coefficient decreases slightly with increasing load.

The analytical functions of approximating the experimental results are used to calculate the energies stored during loading, consumed during unloading, energy losses through hysteresis and energy during the creep period.

The material of the solder alloy mentioned above has a ductile behavior and rheological behavior of visco-elasto-plastic type.

According to the experimental results, the SAC 305 lead-free solder alloy has a higher hysteretic damping coefficient than the copper layer and HASL surface finish.

Chapter 5 entitled "The effect of hysteretic damping of solders on random excitation vibrations" proposes a vibration model with hysteretic damping (Figure 5.1) and analyzes after most cases to determine the transmissibility of the force, the acceleration of the component, the speed spectrum of the response.

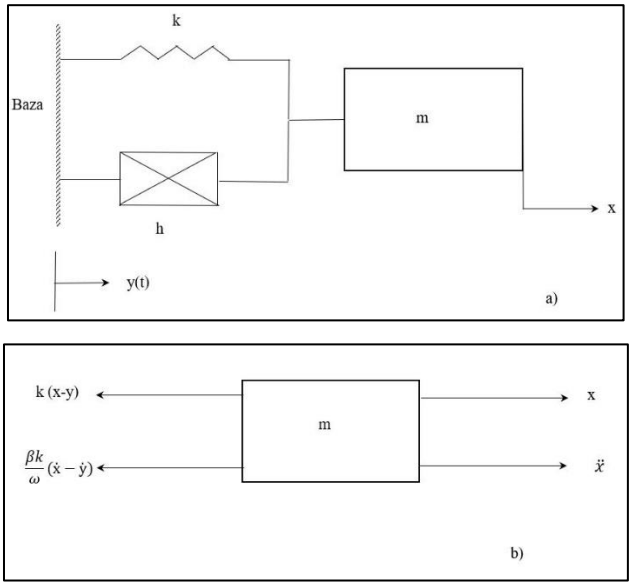

Figure 5. 1. ***Movement pattern with hysteretic damping***

In the equation of motion of an electronic component, the following cases are analyzed:

1. the motherboard oscillates according to a harmonic law
2. the plate oscillates according to the complex harmonic law
3. the plate oscillates according to some deterministic law
4. the plate has random vibrations (t) with the main known statistical parameters (mean, dispersion, centered moments of order 2 and 4).

For the hysterically damped oscillator with harmonic excitation (Figure 5.3), the transmittance of the force is defined as:

$$T_F = \frac{F_t}{F_y} = \frac{m\,\omega^2 X}{kY} = r^2 \left[\frac{1+\beta^2}{(1-r^2)^2+\beta^2}\right]^{1/2}. \qquad (5.1)$$

where $F_t = m\omega^2 X$ is the amplitude of the force transmitted by the solder, $F_y = kY$ the maximum elastic force of the oscillating plate, ω frequency, r the relative frequency (pulsation), Y the amplitude of the plate, k the rigidity, β the hysteretic amorphous coefficient.

The graphs of force transmissibility show the favorable effect of hysteretic damping, as a material property, on the reduction of the force in the weld.

For the spectral oscillation plate, the velocity spectrum of the excitation response ($\ddot{y}(t)$) is defined as the maximum of the function modulus ($\dot{z}(t)$) or in dimensionless coordinates $|\dot{z}(\tau)|$. It is found that this maximum is:

$$S_{v_a} = |\dot{z}(\tau)|_{max} = \left| \frac{e^{-(\frac{\beta}{2r})\tau}}{\sqrt{1-\beta^2/(4r^2)}} \sqrt{P^2+Q^2} \right|_{max} \quad ; \qquad (5.2)$$

Thus the speed is:

$$z_{v_a} = \dot{z}_a(\tau) = \frac{\dot{z}(t)}{Y\omega_n} = \frac{e^{-(\frac{\beta}{2r})\tau}}{\sqrt{1-\beta^2/(4r^2)}} \sqrt{P_a^2+Q_a^2} \sin\left[\sqrt{1-\beta^2/(4r^2)}\,\tau - Q\right] \quad ; \qquad (5.3)$$

From equation (5.47) it is observed that the dimensionless velocity is a function of time τ, hysteretic damping β and relative pulsation r.

Figure 5.8 shows the velocity modulus over time, for different dampings β and pulsations r.

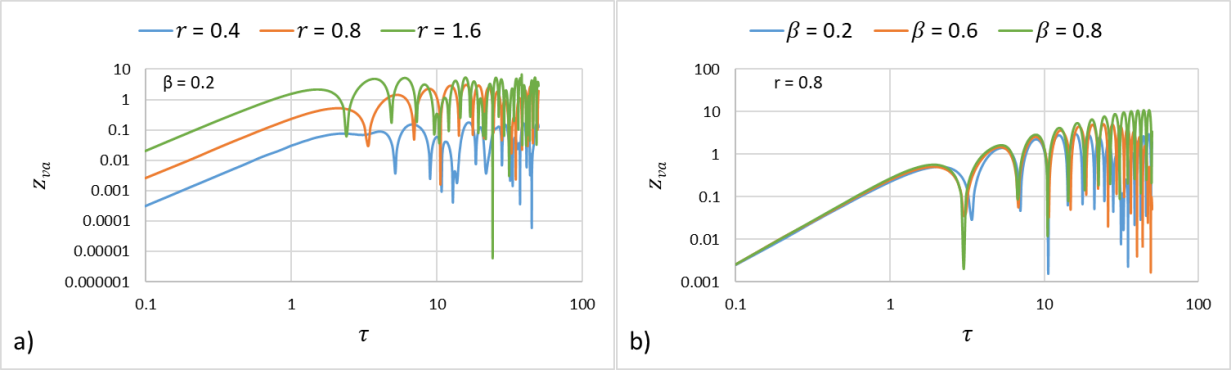

Figure 5. 8. ***Dimensional speed for different pulsations (a) and for different dampings (b)***

The maximum value of the excitation velocity modulus defines the velocity spectrum.

To estimate the life of solders for the random excitation board, a summary analysis of the most used voltage-frequency methods and the recommendation of a method for SAC solders used for different electronic components is proposed.

To characterize the random variable voltage (s) as a function of frequency (f), the power spectral density function - PSD – (S_{ss}) is used to determine the spectral moments m_i:

$$m_i = \int_0^\infty f^i S_{ss}(f)df \quad , \qquad (5.4)$$

with $f = \omega/2\pi$.

To exemplify the specific quantities of the methods of frequency analysis of a random vector recorded over time, the acceleration spectrum of the chassis of an automatic washing machine is used. The experiments are performed in the laboratory of the OMT department of UPB. Power spectral density function ($S_{aa}(\omega)$):

$$S_{aa}(\omega) = \begin{cases} 2PSD_a(\omega) & dacă\ \omega > 0 \\ PSD_a(0) & dacă\ \omega = 0 \end{cases}, \quad (5.5)$$

where $PSD_a(\omega)$ is the function of spectral density, defined with the Fourier transform ($cfft(a)$), the function in the Mathcad program library14.

Figure 5.11 shows the spectral density function of the chassis acceleration, a function specific to the determination of fatigue cycles.

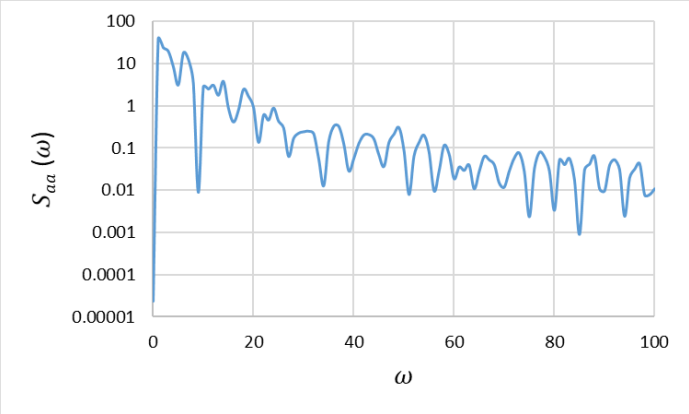

Figure 5. 11. ***Chassis acceleration spectral density function***

For the case of the automatic washing machine, the analysis of the values of the skewness and kurtosis coefficients shows that the acceleration variable is not Gaussian, but falls within the limit, according to the Benasciutti diagram, in a distribution that can be equated by transforming Winterstein into Gaussian distribution. The acceleration vector iteration a_3 is accepted as a Gaussian random vector.

The speed spectrum is determined by the maximum value of the excitation speed mode.

Based on the theoretical model, it was possible to determine the spectral density function of the chassis acceleration of a washing machine which is a specific function for determining fatigue cycles.

It was found from the graph of the transmittance of the force, that the favorable effect of hysteretic damping on the reduction of the force of the solder alloy that forms the solder. The higher the damping coefficient (β), the lower the maximum transmissibility of the force from the exciter plate to the component.

In the case of the plate with spectral oscillations it is observed that if the pulsation increases and the dimensionless velocity is higher, and the damping coefficient (β) changes the evolution over time of the dimensionless velocity, the increase of the damping coefficient (β) leading to a higher amplitude of its variation.

In Chapter 6, entitled "Example. Conclusions. Contributions. Perspectives ", in the example part, choose the case of the TO-5 transistor (NPN BC 337 T5) which is considered similar to a horizontal bar consisting of three cylindrical terminals (bar embedded in the plate by soldering and tip stress) figure 6.2. The transistor is soldered with SAC 305 alloy on a PCB board. To reduce the effect of soldering temperature during installation, the transistor is placed at a distance of 6.35 mm in a plastic tube.

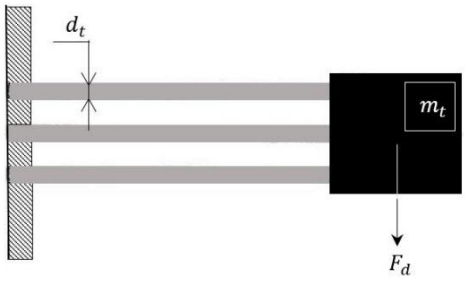

Figure 6. 2. ***Mechanical charging scheme of the TO-5 transistor***

The terminals of the transistor are glued to the board, according to the diagram in figure 6.3. Each of the three terminals is statically required by 1/3 of the transistor weight.

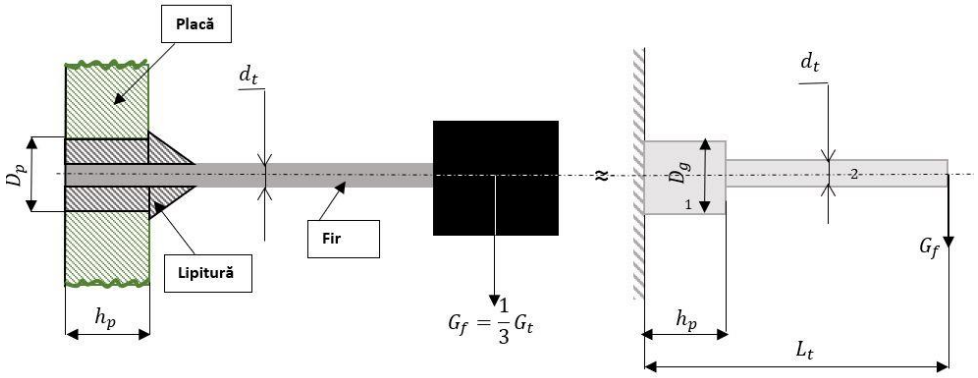

Figure 6. 3. ***Mechanical charging scheme of the TO-5 transistor***

The terminal of negligible weight is embedded by gluing in the plate of thickness h_p and with holes of diameter D_p. The terminal is statically stressed by a force $G_f = (1/3) \cdot G_t$, where G_t is the weight of the transistor. The force is applied at the free end at the distance L_t (terminal length).

By soldering, the terminal becomes a bar with two circular sections 1 and 2 of diameters D_g and d_t and lengths h_p respectively ($L_t - h_p$) at the free end), the deformations including the maximum embedded deformation (δ_{st}) are determined by superimposing the effects generated by the force G_f.

In order to generalize the results regarding the behavior of the transistor with the terminals glued on the board, dimensioning is done for: relative length of the terminal, relative thickness of the terminal, relative moment of inertia of the terminal, dimensionless arrow, dimensionless geometric parameter of the transistor, and with these dimensionless parameters : arrow (w_A), slope (angle) of the deformed middle fiber, arrow determined by the slope, arrow w_{B2a}.

The natural frequency of the transistor with the terminals glued to the board is:

$$f_{ntp} = \frac{1}{2\pi} \sqrt{\frac{g}{\delta_{stt}}} \tag{6.2}$$

where δ_{stt} is the static deformation of the transistor-solder assembly.

In figure 6.6 the variation of the natural frequency of the transistor with the terminals glued in the plate, as a function of the relative length of the terminals (L_a), for different values of the geometric parameter Φ_t figure 6.6.a and different lengths of the terminals L_t figure 6.6.b.

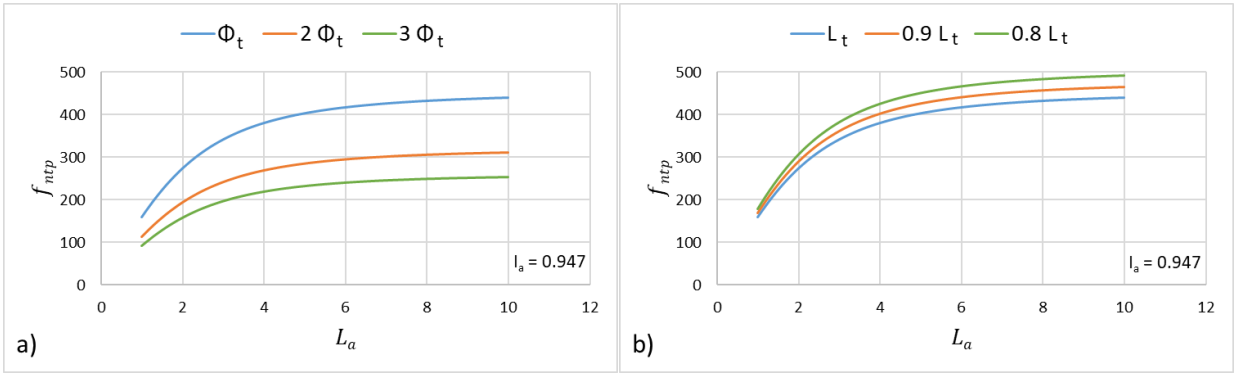

Figure 6. 6. ***Variation of the natural frequency of the TO-5 transistor with the geometric parameter Φ_t (a) and their terminal length (b)***

For the geometric data and the material characteristics of the terminals of the TO-5 transistor, the eigenfrequency with glued terminals and with the consideration of the soldering, is $f_{nTO5} = 382{,}26\ Hz$.

Taking into account the equivalent stiffness k_t of the transistor glued to the plate through the holes and the hysteretic damping, the oscillating system can be considered with a degree of freedom (figure 6.8).

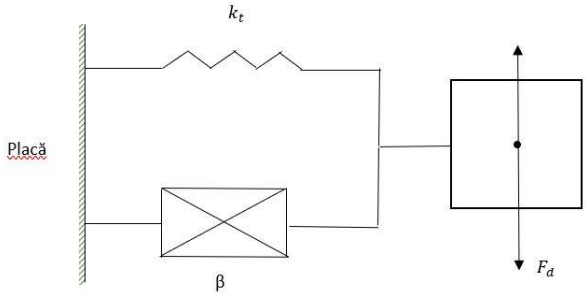

Figure 6. 8. ***Diagram of the TO-5 transistor as an oscillating mechanical system***

For the chosen example, transistor T0-5, the plate transmissibility is determined for the following cases:

1) The plate oscillates harmoniously

2) Plate with complex harmonic oscillation

3) Plate with random oscillation

Determining the bending stresses that appear in the terminals in the embedded area by gluing in the plate as:

$$s_1 = \pm \frac{M_i}{3W_{if}} = \pm \frac{F_d(L_t - h_p) \cdot 32}{3\pi d_t}. \qquad (6.1)$$

Shear stresses occurring in the tubular weld (outer diameter D_p, inner diameter d_t, length h_p):

$$\tau_{fs} = \frac{F_s}{A_s} = \frac{M_i/d_t}{\pi d_t h_p} = \frac{F_d(L_t - h_p)}{\pi {d_t}^2 h_p}. \quad (6.2)$$

Figure 6.11 a, b shows the variations of the bending stresses in the terminals and the shear stresses in the solders as a function of the spectral power of the plate acceleration for different hysteretic damping.

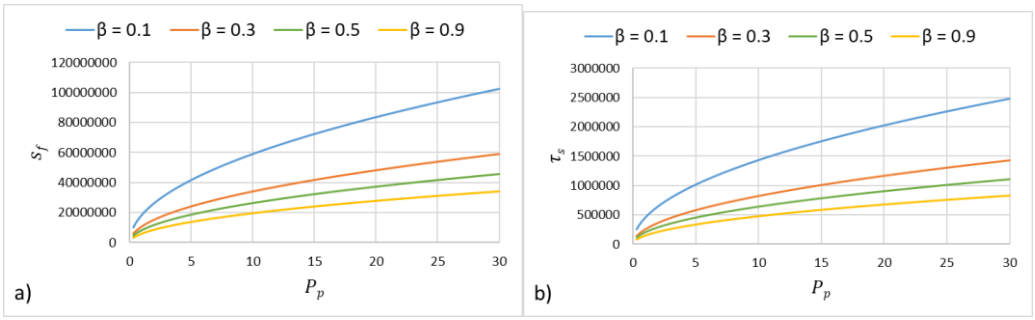

Figure 6. 11. ***Bending stresses in terminals (a) and shear stresses in welds (b) depending on the spectral strength of the plate***

Kovar material fatigue data are used to determine the terminal durability of the transistor [120].

Figure 6.13 illustrates the evolution of the number of cycles to fatigue rupture (durability N_c) depending on the plate acceleration (A_t) for different hysteretic damping (β).

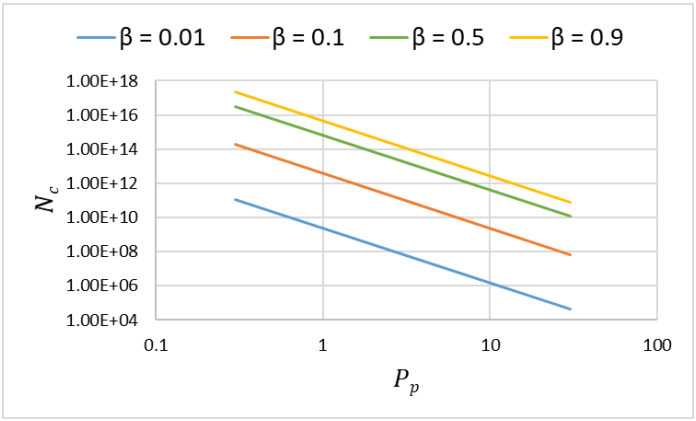

Figure 6. 13. ***Durability of TO-5 transistor terminals depending on the board acceleration***

For soldering the terminals in the plate with SAC soldering alloy, the diagram taken from Ladani's 2009 tests is accepted [87] and by analyzing the graph by points and accepting an exponential law, it is possible to determine the exponent b and the coordinates of a specific point, for example a point 1 ($N_{c1} = 18$ and $\tau_1 = 32\ MPa$) and another point 2 with the coordinates ($N_{c2} = 3000$ and $\tau_2 = 24\ MPa$). In this case it results in $b_{SAC} = 3{,}8$.

The number of solder damage cycles to the terminals of the TO-5 transistor is determined by a ratio of type (6.29):

$$N_{c\tau} = N_{c1}\left(\frac{\tau_1}{\tau}\right)^{b_{SAC}} = 10^3\left(\frac{32}{\tau}\right)^{3.8} \quad (6.3)$$

Taking into account the expression of the shear stresses in the solder, the dependence of the number of cycles ($N_{c\tau}$) on the natural frequency (f_n), on the function of the spectral density of the plate acceleration (P_b) and on the hysteretic damping (β) results. The solder durability of the TO-5 transistor in figure 6.16 as a function of the spectral power of the board acceleration.

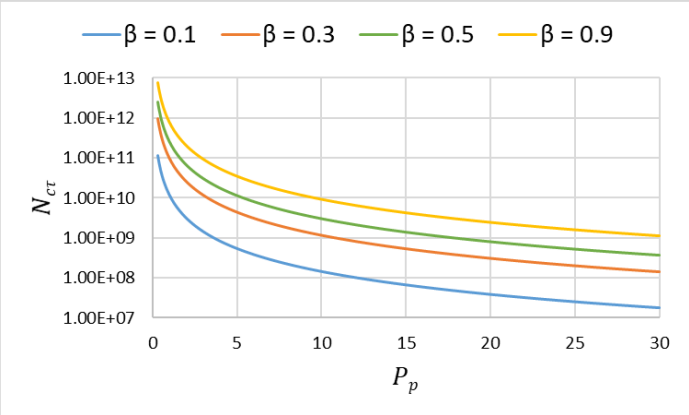

Figure 6. 16. ***Durability of TO-5 transistor terminals depending on the board acceleration***

Conclusions

Following the dimensioning in the theoretical model, the total arrows and those in the points of the transistor scheme were obtained.

As the damping coefficient (β) increases, both the bending stresses in the terminals and the shear stresses decrease. At the same time, the increase of the spectral power leads to the increase of the tensions.

The durability of the transistor terminals increases with increasing hysteretic damping coefficient (β) and decreases as the spectral power of the board increases.

From the analysis of the example applied for the TO-5 transistor, it can be seen that the durability of its solders increases with the increase of the hysteretic damping coefficient (β).

General conclusions

The share of solder defects in electronic equipment is about 70%, and of these defects, about 20% is due to the phenomenon of fatigue, generated by vibrations.

The reduction of the mechanical characteristics with the increase of the temperature, the shear resistance to bending, makes the thermal regime to be the main cause of the reduction of the reliability of the solders and layers (55%).

The phenomena of mechanical hysteresis, creep and relaxation are essential for the study of the fatigue of solders and layers in electronics.

The theoretical and experimental curves with respect to the penetration of the solder and the layer, respectively, confirm the visco-elasto-plastic behavior with high deformation creep.

The force-penetration function for the copper layer deposited on the plate is dependent on the thickness of the layer and the elastic properties of the layer penetrator and the support. The relative thickness of the layer relative to the contact radius (H) defines the layer as a thin layer when H <1.5 and a thick layer when H≥1.5.

An iterative numerical solution for the contact radius - penetration dependence is proposed (figure 2.18).

Based on the diagram of the creep indentation process, the theoretical coefficients of hysteretic damping are determined, considering the deformation at discharge as elastic.

The service life of solders in electronic equipment is determined based on the mechanical criterion (fatigue due to accumulations of plastic deformations).

The constitutive equation of SAC type materials changes with the number of stress cycles.

Simultaneous measurement of normal force, speed, tangential force and acoustic emission, allows the correlation of specific parameters (coefficient of friction at scratch), rigidity, deformation speed and creep at penetration.

The repeatability of the results was verified with the Kolmogorov - Smirnov stratification test. The coefficient of variation is small (4.5% - 5.4%).

For the analysis of the vibration behavior of the electronic components glued on the plate, the one-dimensional movement model of a mass required by inertial forces and bound to the frame by material with elastic and hysteretic behavior is accepted.

The estimation of the solder life on the randomly oscillating plate is done by determining the spectral density (PSD) function of the plate acceleration.

Based on the frequency transfer function of the plate - solder - component system, the dynamic forces in the solder are calculated.

The example of the durability analysis of the TO-5 transistor applies the theoretical part and some experimental results of the present thesis on the mechanical fatigue behavior of solders and their plate binding terminals. Terminals are required for bending the transistor ground and shear soldering.

Contributions

1. Carrying out a complex documentary study for a mechanical-electronic interdisciplinary field.

3. Analysis of the hysteresis phenomenon by indenting the solder materials and the copper layer with HASL type coating with a spherical connected cone (solution for exact indenter and for approximate indentor).

5. The dimensioning of the quantities of interest (force, tensions, deformations) allows the generalization of the theoretical results for any experimental conditions regarding the hysteresis and the creep by indentation.

7. Theoretical and experimental analysis of the instantaneous creep at the end of the load (“bulge effect”).

8. Adaptation of Miner type fatigue models to SAC type materials, taking into account hysteresis losses and creep deformations.

10. Carrying out the test specimens and adapting the experimental methodology to indentation, creep and scratching on the UMT-CETR stand from the Department of Machine Organs and Tribology of the University POLITEHNICA of Bucharest.

11. Statistical analysis of the indentation hysteresis phenomenon in order to identify errors (identical tests) using the Kolmogorov - Smirnov test, proving that the results are repeatable with relatively small errors (6% - 8%).

12. Analysis of the vibratory motion of an electronic component glued to an excitatory plate. The model of rheological behavior of the SAC solder material of type two elements in parallel is accepted (elastic - internal friction).

13. Determination of the dynamic forces in the electronic component for plate with harmonic, complex and random periodic excitation.

14. Analysis of the random vibration characteristics of the component by deducing the transmissibility and spectral power density (PSD) function of the motherboard acceleration. Application for chassis vibrations of an automatic washing machine.

15. Adaptation of identification and monitoring methods in the field of frequency of random cycles with effects on solder fatigue (8 methods).

16. Application of the principle of equivalence of a non-Gaussian vibration spectrum to a Gaussian one for vibrations measured on the chassis of an automatic washing machine.

Perspectives of the paper

The thesis opens new research perspectives in the following directions:

o Simultaneous application of the phenomena of thermal and mechanical fatigue caused by the variation of stresses;

o Equivalence of thermal fatigue with expansion constraints;

o Analysis of the hysteresis phenomenon with temperature variation;

o Experiments on electronic devices with identical components distributed differently on the board and glued with SAC type materials.

BIBLIOGRAPGY

[1] *Suganuma K.*, Lead-Free Soldering in Electronics: Science, Technology, and Environmental Impact, 0 ed. CRC Press, 2003.

[2] *Licari J. J.* și *Swanson D. W.*, Adhesives technology for electronic applications: materials, processes, reliability. Norwich, NY: William Andrew Pub, 2005.

[24] *Coombs C. F.*, „Printed Circuits Handbook”, vol.6, p. 1633.

[39] *Subramanya K. P.*, *Pandit J. K.*, *Prasad C. S.*, și *Thyagaraj M. R.*, „Vibration Analysis Study of Spacecraft Electronic Package: A Review”, **vol. 3**, nr. 3, p. 5, 2014.

[63] *Hills D. A.*, *Nowell D.*, și *Sackfield A.*, Mechanics of elastic contacts. Oxford [England] ; Boston: Butterworth-Heinemann, 1993.
[66] *Johnson K. L.*, Contact mechanics. Cambridge [Cambridgeshire] ; New York: Cambridge University Press, 1985.
[83] *Cutiongco E. C.*, *Vaynman S.*, *Fine M. E.*, și *Jeannotte D. A.*, „Isothermal Fatigue of 63Sn-37Pb Solder”, J. Electron. Packag., **vol. 112**, nr. 2, pp. 110–114, iun. 1990.
[84] *Han J. et al.*, „Experimental study on vibration and sound radiation reduction of the web-mounted noise shielding and vibration damping wheel”, Noise Control Eng. J., **vol. 62**, nr. 3, pp. 110–122, mai 2014.
[85] *Shi X. Q.*, *Zhou W.*, *Pang H. L. J.*, și *Wang Z. P.*, „Effect of Temperature and Strain Rate on Mechanical Properties of 63Sn/37Pb Solder Alloy”, J. Electron. Packag., **vol. 121**, nr. 3, p. 179, 1999.
[87] *Ladani L.* și *Dasgupta A.*, „A meso-scale damage evolution model for cyclic fatigue of viscoplastic materials”, Int. J. Fatigue, **vol. 31**, nr. 4, pp. 703–711, apr. 2009.
[88] *Zhang Q.*, *Dasgupta A.*, și *Haswell P.*, „Partitioned viscoplastic-constitutive properties of the Pb-free Sn3.9Ag0.6Cu solder”, J. Electron. Mater., **vol. 33**, nr. 11, pp. 1338–1349, nov. 2004.
[89] *Tudor A.* și *Vlase M.*, Uzarea Materialelor, Bren. 2010.
[105] *Chisiu G.* și *Tudor A.*, „Wear characteristics of uhmw polyethylene by scratching method”, Journal of the Balkan Tribological Association, Vol. 20, Nr. 1, 2014, p. 14.
[106] *Petrescu A. M.*, *Paduraru G. I.*, *Tudor A.*, și *Alexandru N.*, „MECHNANICAL TESTING OF ELECTRONIC PRINTED CIRCUIT BOARDS AND SOLDERING ALLOYS”, Tehnol. Inov. - Rev. Construcţia Maşini, nr. 2–3, p. 4, 2015.
[107] *Petrescu A. M.*, *Stoica N. A.*, *Tudor A.*, *Rădulescu A. V.*, *Stoica M.*, și *Chişiu G.*, „Micro-scratching tests of a lead-free solder alloy SAC 305 used in electronic industry”, IOP Conf. Ser. Mater. Sci. Eng., **vol. 514**, p. 012015, iun. 2019.
[120] *Steinberg D. S.*, Vibration analysis for electronic equipment, 3rd ed. New York: John Wiley & Sons, 2000.